Progress In Electromagnetics Research B, Vol. 62, 277–288, 2015

On the Optimization of Halbach Arrays as Energy Storage Media

Daniel Månsson*

Abstract—In the paper presented here the optimization of Halbach arrays as storage media for mechanical potential energy is investigated with numerical simulations using FEMM and analytical calculations using the Maxwell stress tensor. Two opposing Halbach arrays form a "magnetic spring" and mechanical potential energy is stored when this structure is compressed. It is here seen that the wavelength of the magnetization in the material and the dimensions greatly influence the stored energy density. A clear region of maximum is identified which leads to important conclusions on how the material should be employed. The suggested approach for storing energy have advantages and approximately 250 kJ/m^3 can be reached. The main drawback is the large prize of rare earth metals such as Neodymium.

1. INTRODUCTION

With the threat of climate change and a depleting stock of non-renewable fossil fuels and other valuable resources the improved energy efficiency on all levels of society is of great interest. The dominant energy carrier today is electricity and without it the modern world would collapse. Logically, this leads to the conclusion of a, on several levels, better power grid. Therefore, the concept of a "smart grid" has been suggested and it is the topic of much research today. A smart grid incorporates (to a much larger extent than most current power grids) information and communication technology (i.e., ICT), distributed renewable energy production and energy storage. The ICTs will, for instance, come in the form of "smart appliances", e.g., energy demanding household systems (e.g., washing machines) that can be controlled to only be active at times of a surplus of cheap and "clean" energy.

The current forms of large power generation with, e.g., coal, nuclear or hydro power, will be supplemented with renewable energies through, e.g., wind, solar, geothermal, in which the production will be distributed over the geographical area of concern. However, these renewable energy sources are stochastic with time and, therefore, the peak energy availability in, e.g., the solar intensity or wind speed, may not coincide with the peak energy demand. Thus, the energy produced must be stored in an intermediary state in wait for the demand to increase. The stored energy can be in the form of chemical energy in batteries, potential energy of elevated water in a basin (i.e., pumped hydro), electromagnetic energy in the charge of a capacitor, kinetic energy in the momentum of a flywheel etc. (see, e.g., [1–3]).

In addition, the concept of the prosumer (i.e., producer-consumer) [4] is vital. An example of this is a residential home with renewable energy production (e.g., through wind or solar power) with an energy storage system that can store, and return to the grid, surplus energy that is currently not in demand locally. The local energy demand is obtained through smart meters [5] and other measurements of the power consumed locally by devices and equipment. This information is used to determine the surplus, or deficit, of power available locally where a surplus can be returned to the grid. Likewise, it is important to realize that energy storage systems act as stabilizers in the grid and can, e.g., support a strained generation if the load is high. Different financial schemes for energy return or small scale energy production is discussed and tested around the globe today.

Received 11 February 2015, Accepted 3 April 2015, Scheduled 16 April 2015
* Corresponding author: Daniel Månsson (manssond@kth.se).
The author is with Electromagnetic Engineering Lab, School of Electrical Engineering, Royal Institute of Technology KTH, Sweden.

A fundamental, but crucial, point for the prosumer is that there is a reliable, safe and, both electrotechnical and financially, effective method of storing energy in an intermediate form to balance the energy surplus or deficit. Large scale energy storage has already existed for a relatively long time in power grids, e.g., pumped hydro storage. More novel methods with, e.g., compressed air energy storage (CAES), large arrays of flywheels or superconducting coils as the storage media have also been investigated and/or introduced.

An energy storage system can operate in three different states; charging, storing and discharging. Examples of important parameters for investigating and comparing different energy storage media are:

- Energy storage capability (e.g., volume energy density [J/m^3] or mass energy density [J/kg]).
- Charge and discharge times ([s]).
- Charge and discharge depths ([%]).
- Unit energy stored per capital cost (e.g., [J/€]).
- Conversion losses.

It is important, for the successful implementation of all aspects of the smart grid, to evaluate uncommon and unusual forms of energy storage media and systems. This as all types of energy storage will not be equally suitable for all applications and installations in a smart grid. The needs of, and requirements on, the energy storage system will differ both with the power production used (e.g., photovoltaic cells versus wind power plant) but also with the characteristics of the load (e.g., residential homes compared to apartment buildings or small industries).

For example, energy can be stored mechanically as potential energy through the deformation of a spring from its natural state. Hookes law states that, ignoring permanent mechanical damage, a compressed spring stores potential energy (work) equivalent to the amount of work carried out against the restoring force of the spring ($\mathbf{F}_{spring} = -kx'\hat{\mathbf{x}}$ if the applied force, $\mathbf{F}_a$, is in the $\hat{\mathbf{x}}$ direction) along the path of compression. If a spring is compressed a distance x from its natural (i.e., relaxed) length, the work performed by the outside agent is $W_a = \int_0^x \mathbf{F}_a \cdot d\mathbf{x}'$. Then, if the spring is not damaged, the magnitude of the applied force is equal to the restoring force of the spring ($|\mathbf{F}_a| = |\mathbf{F}_{spring}|$) and all of the applied work is stored.

$$W_{stored} = -W_a = -\int_0^x F_{spring}\, dx' = \int_0^x (kx')\, dx' = \frac{1}{2}kx^2 \tag{1}$$

The minus sign in (1) arises as work has to be expended against the restoring force of the spring to compress it and the energy stored in the spring after compression is positive (can be used for positive work at a later time).

Neodymium magnets ($Nd_2Fe_{14}B$) are widely used today for a wide variety of purposes and some commercial types have an adhesive force of approximately 100 kg even though the dimensions are only $5 \times 5 \times 2.5$ cm and for smaller magnets of 1 cm^3 the force could be almost 4 kg [6]. Therefore the idea of using permanent magnets as springs isn't uncommon and, thus, as media for energy storage is not inconceivable. In a previous paper the suitability of such a magnetic energy storage system was studied [7] and the general conclusion was that there are some areas and applications for which it could be suitable. It was observed that 1.) losses due to induced eddy currents are negligible, 2.) the magnetic structures are not at risk of demagnetization, 3.) the temperature increase in the material is negligible and 4.) the internal stress forces are manageable. In the work presented here the previous paper will be expanded upon to investigate the optimization of the energy stored in such a storage system using so called *Halbach* arrays.

The analytical investigations presented here were augmented with results using the software *FEMM* [8] ("Finite Element Method Magnetics") and it has previously shown itself to be an accurate tool [9]. However, as with all numerically simulated results, the finer details of the quantities (e.g., the magnetic flux densities, **B** fields) can always be associated with errors due to, e.g., mesh size and/or the actual method being used. Also, it should be mentioned that FEMM only offers a "2.5D approach (i.e., not "true" 3D). This means that the numerical simulations do not, per see, include edge effects from fields in the "depth dimension", but they do take the depth of the structure into account for the total computed quantity (e.g., force, energy etc.). In addition, the general field structures were

confirmed (but not shown here) with another field simulation software (*Vizimag* [10]). Using FEMM, the magnetic forces are first calculated for the different cases of interest and these are then integrated over the different gap lengths to yield the stored energies. Finally, for the numerical values presented here (see Figs. 4–7) material with residual magnetization (i.e., *remanence*), B_r, of approximately 1.3 T and with relative permeability $\mu_r = 1.5$ [6] (corresponding to N42 type graded NdFeB) was considered. This is considered to be a realistic choice of material (see [7] for a discussion on the material).

2. HALBACH ARRAYS

2.1. Introduction

The phenomenon of having a one-sided flux from a structure was originally described by John C. Mallinson in 1973 [11]. He investigated the effects of having a cuboid body with a magnetization in the material that was continuously rotating from one end to the other. Later, in 1981, this phenomenon was realized with individual magnets by Klaus Halbach [12] whose name is used to describe the structures. The difference in the field expressions deduced below (e.g., (8) and (11)) is only the term $\frac{\sin(\epsilon\pi/m)}{\pi/m}$ that describes the discretization (where the width of a single magnet is given by $\frac{\epsilon\lambda}{m}$). In [13] an excellent online demonstration tool, showing the magnetic field created by a discrete Halbach array, can be found. As shown in Fig. 1 a discrete Halbach array be can made continuous by decreasing the width of individual magnets and at the same time decrease the rotation speed of the direction of magnetization in individual magnets, i.e., increasing m (the number of magnets per wavelength). This is the same as having

$$\lim_{m\to\infty} \frac{\sin(\epsilon\pi/m)}{\pi/m} = 1 \tag{2}$$

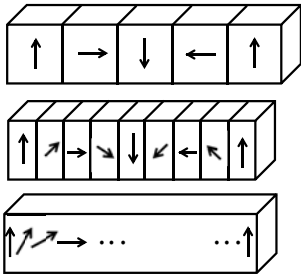

Figure 1. Two discrete (with $m = 5$ and $m = 9$, respectively) and one continuous (bottom) Halbach array. The wavelengths of the magnetization are in all the three cases equal to the individual widths of the arrays.

As is shown in [7] a discrete Halbach array can, quite easily, be made to approximate a continuous one very well. Thus, in the analyses to follow below, we assume a continuous magnetization with the knowledge that this can be constructed, and convincingly approximated, by discrete magnets.

Some common applications for Halbach arrays are:

1. as "wigglers"/"undulators" in free-electron lasers,
2. in high-speed trains with magnetic levitation,
3. magnetic bearing in flywheels,
4. in brushless motors.

Here, two Halbach arrays are utilized, in a dual configuration, as a magnetic spring. Mechanical work is expended when this is compressed by a motor and the energy is stored in this compressed state. The energy can later be used when the "spring" is released and the upward motion drives a generation.

2.2. Magnetic Field from Single Halbach Array

The deduction below gives the magnetic field ($\mathbf{H}$) from a body with direction of magnetization in the material that is continuously rotating as a function of the width. Assume that a cuboid stretches out in the xz plane and is situated with its top surface at $y = 0$ and the bottom surface at $y = -\beta$ (i.e., β is the height of the cuboid). The magnetization is given by (with $M_z = 0$)

$$\mathbf{M} = M_0 \left(\hat{\mathbf{x}} \sin kx + \hat{\mathbf{y}} \cos kx\right) \tag{3}$$

This will give an enhancement of the field on the lower surface of the cuboid. Here, k is the wavenumber, i.e., $k = \frac{2\pi}{\lambda}$ and λ is the wavelength of the Halbach array. (λ is twice the *pole pitch*, i.e., the distance between two consecutive poles.) The magnetic flux density, $\mathbf{B}$, is given by

$$\mathbf{B} = \mu_0 \left(\mathbf{H} + \mathbf{M}\right) \tag{4}$$

Since $\nabla \cdot \mathbf{B} = 0$ we have that

$$\nabla \cdot \mathbf{H} = -\nabla \cdot \mathbf{M} \tag{5}$$

Also, as for a permanent magnet there are only bound magnetic currents we have $\mathbf{J}_{free} = 0$ and, thus, $\nabla \times \mathbf{H} = 0$. We can therefore describe the magnetic field with the magnetic scalar potential alone [14] $\mathbf{H} = -\nabla\phi$ and we get (minus signs canceling)

$$\nabla \cdot \mathbf{M} = \nabla \cdot \nabla\phi = \nabla^2\phi \tag{6}$$

Using the given magnetization for the structure (i.e., (3)) together with necessary boundary conditions the scalar potential can be found to be [15]

$$\left.\begin{aligned} \phi_{above} &= 0 \\ \phi_{inside} &= \frac{M_0}{k}\left(e^{ky} - 1\right)\cos kx \\ \phi_{below} &= \frac{M_0}{k}\left(1 - e^{k\beta}\right)e^{ky}\cos kx \end{aligned}\right\} \tag{7}$$

We can now express the magnetic field through $\mathbf{H} = -\nabla\phi$ in the different regions but we are here only interested in the enhanced field below the cuboid (as $\mathbf{H}_{above} = 0$)

$$\mathbf{H}_{below} = M_0\left(1 - e^{k\beta}\right)e^{ky}\left[\hat{\mathbf{x}}\sin(kx) - \hat{\mathbf{y}}\cos(kx)\right] \tag{8}$$

(M_0 is the maximum magnetization which is related to the residual magnetism in the material through $M_0 = \frac{B_r}{\mu_0\mu_r}$ [16]). Thus, in the next section concerning the dual Halbach configuration, these fields originates from the upper Halbach array. If the magnetization in the material is changed to (still with $M_z = 0$)

$$\mathbf{M}' = M_0 \left(\hat{\mathbf{x}} \sin kx - \hat{\mathbf{y}} \cos kx\right) \tag{9}$$

the magnetic field is flipped so that it is canceled below the cuboid and enhanced above it. The magnetic scalar potential then becomes

$$\left.\begin{aligned} \phi'_{above} &= \frac{-M_0}{k}\left(1 - e^{-k\beta}\right)e^{-ky}\cos kx \\ \phi'_{inside} &= \frac{M_0}{k}\left(e^{-k(\beta+y)} - 1\right)\cos kx \\ \phi'_{below} &= 0 \end{aligned}\right\} \tag{10}$$

The enhanced magnetic field above the cuboid becomes ($\mathbf{H}'_{below} = 0$)

$$\mathbf{H}'_{above} = -M_0\left(1 - e^{-k\beta}\right)e^{-ky}\left[\hat{\mathbf{x}}\sin(kx) + \hat{\mathbf{y}}\cos(kx)\right] \tag{11}$$

Thus, in the next section concerning the dual Halbach configuration, these primed fields originates from the lower Halbach array. It is important to remember that these expressions are only valid above and below the Halbach arrays, i.e., the do not give any information about the fields on the vertical sides, which is one reason for why numerical simulations with FEMM is also used.

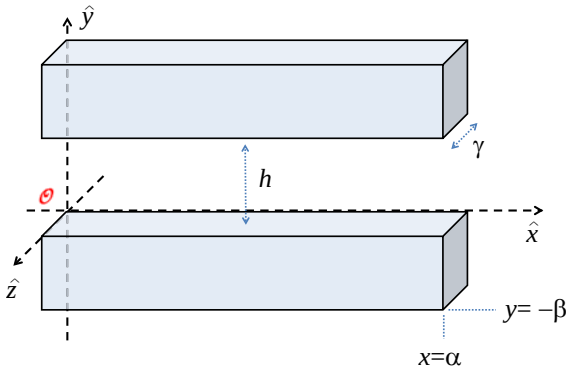

Figure 2. Two Halbach arrays with opposing magnetization (e.g., "North-North") is used in a dual configuration. The two arrays have identical dimensions of α, β and γ (i.e., width, height and depth).

2.3. Magnetic Field from a Dual Halbach Configuration

For use in a energy storage medium two Halbach arrays are used in a dual configuration (see Fig. 2) with a gap distance of h between them. The magnetizations in the two arrays are chosen such that the enhanced fields are towards each other and that the magnetic poles created are the same, thus, repelling each other (i.e., "north-north" or "south-south"). Note that the magnetic fields described above were given for a Halbach array that has its upper surface at $y = 0$, thus, (8) needs to be changed to accurately described the gap distance h. If $\mathbf{X}$ describes a point in a coordinate system that is shifted $\Delta\mathbf{X}$ compared to another coordinate system, in which $\mathbf{X}_0$ describes the same point, we have $\mathbf{X} = \mathbf{X}_0 - \Delta\mathbf{X}$. Therefore, for the upper Halbach array we have to substitute y with $y - (h + \beta)$ in (8). Using this substitution, the magnetic field below the upper Halbach array becomes

$$\mathbf{H}_{below,shifted} = M_0 \left(1 - e^{k\beta}\right) e^{k(y-(h+\beta))} \left[\hat{\mathbf{x}} \sin(kx) - \hat{\mathbf{y}} \cos(kx)\right] \tag{12}$$

Putting the top surface of the lower Halbach array at $y = 0$, the total magnetic field (i.e., (12) + (11)) in the region between the arrays (i.e., $y = (0, h)$) becomes

$$\begin{aligned} \mathbf{H}_{tot} = {} & M_0 \sin(kx) \left[\left(1 - e^{k\beta}\right) e^{k(y-(h+\beta))} - \left(1 - e^{-k\beta}\right) e^{-ky}\right] \hat{\mathbf{x}} \\ & - M_0 \cos(kx) \left[\left(1 - e^{k\beta}\right) e^{k(y-(h+\beta))} + \left(1 - e^{-k\beta}\right) e^{-ky}\right] \hat{\mathbf{y}} \end{aligned} \tag{13}$$

Observe, that in this paper it is assumed that the dimensions (i.e., α, β and γ) of the two individual Halbach arrays are equal. In particular, non-equal widths would create torques on the arrays and, thus, decrease the stored potential energy. In addition, the wavelengths of the magnetization in the two arrays are considered to be the same as as this also was seen (but not shown here) to decrease the stored energy.

Finally, note that the here derived magnetic fields were plotted and compared, with excellent agreement, with simulated results but this is not explicitly shown here.

3. CALCULATING THE ENERGY STORED VIA MAXWELL'S STRESS TENSOR

Armed with (13) we can investigate the energy stored in the dual configuration. When the two arrays are brought together, i.e., h in (13) is decreased, it is similar as to pressing together a mechanical spring (i.e., increasing x in (1)). Therefore, we need to look at, e.g., the force on the lower Halbach array when h is decreased (keeping the lower array fixed), which is best done by using *Maxwell's stress tensor*, $\mathbb{T}$ [14]. (It should be noted that there are several other ways of calculating magnetic forces, e.g., with the *Biot-Savart law*, but according to [17] Maxwell's stress tensor is preferable.) Here, Maxwell's stress tensor only contains components of the magnetic field as the electric field is inherently zero for stationary permanent magnets and it has been shown that the effect of $d\mathbf{B}/dt \neq 0$ is negligible (see

below or [7] for a discussion on the effects of *eddy currents* created via $\nabla \times E = -d\mathbf{B}/dt$). Thus, the stress tensor reduces to

$$T_{ij} = \frac{1}{\mu_0}\left(B_i B_j - \frac{1}{2}\delta_{ij}B^2\right) \tag{14}$$

where the indices i and j refer to the x, y or z components of the field, δ_{ij} is the Kronecker delta (i.e., $\delta_{xx} = \delta_{yy} = \delta_{zz} = 1$ and zero otherwise) and $B^2 = B_x^2 + B_y^2 + B_z^2$. The individual tensor elements, T_{ij}, can be viewed as the force (per unit area) in the ith direction acting on a surface element having its normal in the jth direction. Thus, the terms T_{xx}, T_{yy} and T_{zz} represent pressures and the other six terms (T_{xy}, T_{xz}, etc.) represent shearing forces.

The total force on an object is, according to Newton's second law, given by the time rate of change of the momentum of the object [14]:

$$\mathbf{F} = \frac{d\mathbf{p}_{mech}}{dt} = -\epsilon_0\mu_0\frac{d}{dt}\int_v \mathbf{S}\, d\tau + \oint_S \mathbb{T}\cdot d\mathbf{a} \tag{15}$$

As mentioned above, the electric field is zero or negligible and therefore the poynting vector is $\mathbf{S} = \mathbf{E}\times\mathbf{H} = 0$ and the first volume integral (representing the momentum stored in the electromagnetic fields themselves) vanishes. The force on the object can now be described with the closed surface integral alone.

$$\mathbf{F} = \oint_S \mathbb{T}\cdot d\mathbf{a} \tag{16}$$

where $d\mathbf{a} = \hat{\mathbf{n}}da$ and $\hat{\mathbf{n}} = n_x\hat{\mathbf{x}} + n_y\hat{\mathbf{y}} + n_z\hat{\mathbf{z}}$ (i.e., the direction of the surface normal will vary over the surface).

For the energy storage investigation, only F_y (i.e., $\mathbf{F}\cdot\hat{\mathbf{y}}$) is of interest to us and it is assumed that the configuration can be made mechanically fixed so that the movement along the $\hat{\mathbf{x}}$ and $\hat{\mathbf{z}}$ directions are zero. However, the effect of internal self-forces are discussed below (see 5.2 and in [7]). The force of interest is $F_y = \oint_S f_y da$ and $f_y da = (\mathbb{T}\cdot d\mathbf{a})\cdot\hat{\mathbf{y}} = (\mathbb{T}\cdot d\mathbf{a})_y$. For the cuboid (see Fig. 3), which is a "discrete" structure, each side i is best handle individually, thus

$$(\mathbb{T}\cdot d\mathbf{a})_y|_{\forall\,\text{sides}\,i\in S} = (\hat{\mathbf{x}}T_{yx,i}\cdot da_{x,i}\hat{\mathbf{x}} + \hat{\mathbf{y}}T_{yy,i}\cdot da_{y,i}\hat{\mathbf{y}} + \hat{\mathbf{z}}T_{yz,i}\cdot da_{z,i}\hat{\mathbf{z}})\,|_{\forall\,\text{sides}\,i\in S} \tag{17}$$

Please note that some terms in (17) are directly zero either due to a necessary field component being zero in that region (e.g., $H_{z,1} = 0 \Rightarrow T_{yz,1} = 0$) or that the surface normal for that side is such that parts of the scalar product becomes zero (e.g., $\hat{\mathbf{n}}_1 = \hat{\mathbf{y}} \Rightarrow d\mathbf{a}_1 = da_1\hat{\mathbf{y}} \Rightarrow (\mathbb{T}\cdot d\mathbf{a})_{y,1} = (\hat{\mathbf{x}}T_{yx,1} + \hat{\mathbf{y}}T_{yy,1} + \hat{\mathbf{z}}T_{yz,1})\cdot da_1\hat{\mathbf{y}} = 0 + T_{yy,1}da_1 + 0$). Each side of the cuboid does therefore not contribute in full to $(\mathbb{T}\cdot d\mathbf{a})_{y,total}$. Using (17) and taking care with the direction of $d\mathbf{a}$ of the individual sides

1. Top, $(\mathbb{T}\cdot d\mathbf{a})_{y,1} = [d\mathbf{a}_1 = da_1\hat{\mathbf{y}}] = da_1T_{yy,1}$.
2. Right, $(\mathbb{T}\cdot d\mathbf{a})_{y,2} = [d\mathbf{a}_2 = da_2\hat{\mathbf{x}}] = da_2T_{yx,2}$.
3. Bottom, $(\mathbb{T}\cdot d\mathbf{a})_{y,3} = [d\mathbf{a}_3 = -da_3\hat{\mathbf{y}}] = -da_3T_{yy,3} = [\text{here}] \approx 0$.

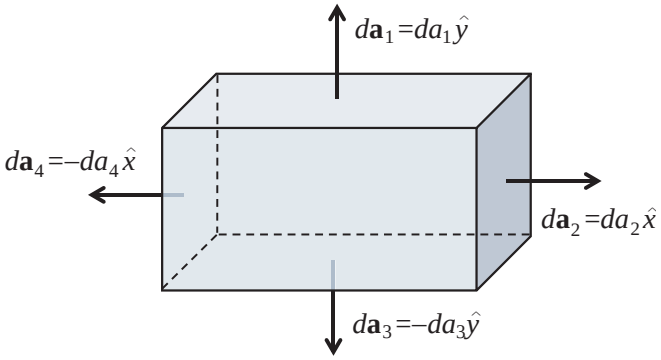

Figure 3. Cuboid with its surface elements for four sides shown representing the lower Halbach array in the dual configuration (for clarity the upper array isn't shown).

4. Left, $(\mathbb{T}\cdot d\mathbf{a})_{y,4} = d\mathbf{a}_4 = -da_4\hat{\mathbf{x}}] = -da_4 T_{yx,4}$.
5. Front (not indexed in Fig. 3), $(\mathbb{T}\cdot d\mathbf{a})_{y,5} = [d\mathbf{a}_5 = da_5\hat{\mathbf{z}}] = da_5 T_{yz,5}$.
6. Back (not indexed in Fig. 3), $(\mathbb{T}\cdot d\mathbf{a})_{y,6} = [d\mathbf{a}_6 = -da_6\hat{\mathbf{z}}] = -da_6 T_{yz,6}$.

This can directly be simplified as that the total magnetic field below the lower array arises from $\mathbf{H}'_{below} = 0$ (ideally) and fields from the upper array, $\mathbf{H}_{below}$, which is $\neq 0$ but very small in this region. In addition, the upper array is shielded from this region by the magnetic material in the lower array. Thus, this part of the surface integral (i.e., "Bottom"), which arises from $T_{yy,3}$, will not, for Halbach arrays, contribute measurably to F_y and this was confirmed via FEMM simulations but is not explicitly shown here.

In addition, the contributions to the surface integral from the right and left side (i.e., from $T_{yx,2}$ and $T_{yx,4}$) were found (but not explicitly shown here) to be negligible. At most these contributions were, for the range of wavelengths, gap lengths and array heights investigated here, approximately 1%. As the analytical expression for the field is not valid in these two regions it was confirmed with FEMM. Similarly the contribution from $T_{yz,5}$ and $T_{yz,6}$ is believed, for the same reasons, to be negligible. However, this can not be tested with FEMM as it is not, as mentioned above, a full 3D solver. All in all, it is believed that the effects from the vertical sides and, even more, edges are small compared to the force in the $\hat{\mathbf{y}}$ direction that arises from the horizontal surfaces. This is a valid belief that will be justified when comparing the analytical calculations with the numerical simulations with FEMM (see Fig. 4).

The simplifications lead to $f_y da = (\mathbb{T}\cdot d\mathbf{a})_y \approx T_{yy,1} da_1$ and the vertical force on the cuboid becomes

$$F_y = \oint_S (\mathbb{T}\cdot d\mathbf{a})_y \approx \int_{top} T_{yy,1} da_1 \tag{18}$$

Furthermore, as $M_z = 0$ and $\mathbf{H}_{tot,1}$ (and, thus, also $T_{ij,1}$) is independent of z, $d\mathbf{a}_1 = da_1\hat{\mathbf{y}} = \gamma dx\hat{\mathbf{y}}$, can be done (where γ is the depth of the Halbach array). Thus, the depths of the arrays only scale the resulting force and only a line integral has to be calculated. The vertical force on the cuboid (i.e., the lower Halbach array) then becomes

$$F_y = \oint_S (\mathbb{T}\cdot d\mathbf{a})_y \approx \int_{top} T_{yy,1} da_1 = \gamma \int_{x=0}^{\alpha} T_{yy,1} dx \tag{19}$$

Using (14) the term $T_{yy,1}$ becomes (observe that here the $\mathbf{B}$ field terms denote the <u>total</u> field, as deduced in (13), in the region between the Halbach arrays and also that $B_z = 0$)

$$T_{yy,1} = \frac{1}{\mu_0}\left(B_y B_y - \frac{1}{2}\left(B_x^2 + B_y^2\right)\right) = \frac{1}{2\mu_0}\left(B_y^2 - B_x^2\right) \tag{20}$$

With (13), and using the fact that $\mathbf{B} = \mu_0\mathbf{H}$ in the gap and that $M_0 = \frac{B_r}{\mu_0\mu_r}$, $T_{yy,1}$ becomes

$$\left.\begin{aligned} T_{yy,1}(x,y) &= \frac{B_r^2}{2\mu_0\mu_r^2}\left(\cos^2(kx)\theta(y) - \sin^2(kx)\psi(y)\right) \\ \theta(y) &= \left(\left(1-e^{k\beta}\right)e^{k(y-(h+\beta))} + \left(1-e^{-k\beta}\right)e^{-ky}\right)^2 \\ \psi(y) &= \left(\left(1-e^{k\beta}\right)e^{k(y-(h+\beta))} - \left(1-e^{-k\beta}\right)e^{-ky}\right)^2 \end{aligned}\right\} \tag{21}$$

To investigate the energy stored when the two Halbach arrays are forced together we look, e.g., at the force on the lower array and, thus, set $y = 0$ (i.e., the remainder of the surface, over which the tensor is integrated, is at the upper boundary of the lower array).

$$\left.\begin{aligned} \theta(0) &= \left(\left(1-e^{k\beta}\right)e^{k(-h-\beta))} + \left(1-e^{-k\beta}\right)\right)^2 \\ \psi(0) &= \left(\left(1-e^{k\beta}\right)e^{k(-h-\beta))} - \left(1-e^{-k\beta}\right)\right)^2 \end{aligned}\right\} \tag{22}$$

With the help of the online mathematical tool *Wolfram Alpha* [18] the line integral (19) becomes

$$\begin{aligned} F_y &= \gamma\frac{B_r^2}{2\mu_0\mu_r^2}\int_{x=0}^{\alpha}\left(\cos^2(kx)\theta(0) - \sin^2(kx)\psi(0)\right)dx \\ &= \begin{bmatrix} c_1 = \theta(0) - \psi(0) \\ c_2 = \theta(0) + \psi(0) \end{bmatrix} = \gamma\frac{B_r^2}{2\mu_0\mu_r^2}\frac{1}{4k}\left(2k\alpha c_1 + c_2\sin(2k\alpha)\right) = \gamma\frac{B_r^2}{2\mu_0\mu_r^2}\left(\frac{\alpha c_1}{2} + \frac{\lambda}{8\pi}c_2\sin\left(\frac{4\pi\alpha}{\lambda}\right)\right) \end{aligned} \tag{23}$$

Now the energy stored becomes (the minus sign arises due to the same reasons as in (1))

$$E = -\gamma \frac{B_r^2}{2\mu_0 \mu_r^2} \int_{h=h'}^{0} \left(\frac{\alpha c_1(h)}{2} + \frac{\lambda}{8\pi} c_2(h) \sin\left(\frac{4\pi\alpha}{\lambda} \right) \right) dh \tag{24}$$

where, the gap size ranges from h' to (ideally) 0. It is important to remember that if the starting gap size isn't infinite then some mechanical work has to be expended to place the respective Halbach arrays at their "starting positions" (i.e., here h'). Also, after compression the "practical" stopping gap size might not be exactly zero. Thus, the stored energy always has to be calculated via the line integral from the starting to the stopping gap size. It could be asked whether the expressions for the magnetic field and, thus, the tensor calculations are valid when the gap size approaches zero. However, as before, the calculations are here justified by the good correspondence with the numerical simulations using FEMM. Special care was taken to have a mesh size, between the Halbach arrays, that gave accurate results even for small gap sizes which was ensured by successively decreasing the mesh size until the simulation results didn't improve further.

The expression for the energy can finally be solved numerically using, e.g., *Matlab* (see [19]) but care must be taken so that the step length in the numerical integration is adequate (i.e., that $\Delta h \approx dh$).

4. OPTIMIZATION OF HALBACH ARRAYS FOR ENERGY STORAGE

Mechanical potential energy, originating from the compression, can be stored in the dual Halbach configuration due to the magnetization in the material and, as can be seen from the derivation above and (24), this energy is dependent on:

- the wavelength of the magnetization (λ),
- the dimensions of the Halbach arrays (α, β and γ),
- the compression length (i.e., from h' to 0),
- material properties of the magnetic structures.

These factors can be understood if the expression for the magnetization is studied (e.g., $\mathbf{M} = M_0(\hat{\mathbf{x}} \sin kx + \hat{\mathbf{y}} \cos kx)$). From this, it can be understood that the total magnetic moment ($\mathbf{m} = \int \mathbf{M} dv$) of the structure will, in some manner, vary periodically with the width (i.e., α) besides being directly dependent on λ via $k = \frac{2\pi}{\lambda}$. As previously discussed, it can safely be assumed that the depth, i.e., γ, only scales the stored energy linearly. However, the height, i.e., β, comes directly into the equations and will strongly influence the stored energy. As can be seen in Fig. 4, β and λ greatly affects the stored energy. Ten values of β, equally spaced from 1 mm to 2 cm, are tested for wavelengths up to twice the width of the array, i.e., $\lambda/\alpha = 2$. The results from the numerical simulations using FEMM (dashed lines with squares) and the analytical calculations using (24) (solid lines with circles) are very similar. Thus, the assumptions and approximations made seem to be valid. Only for $\beta \gtrsim \alpha$ and $\lambda = 2\alpha$ are there large, non-negligible, deviations. However, for $\lambda > \alpha$ the behavior of the magnetic structures starts to to deviate and can no longer be considered to be Halbach arrays (i.e., the $\mathbf{B}$ fields are more similar to that created by "normal" permanent magnets) and, thus, (19) is no longer valid. In fact, the interval of the wavelengths used to calculate the analytical results in Fig. 4 was not continuous. We here introduced the concept of *relative wavelength*, $\lambda_r = 2\frac{\alpha}{N}$, where $N = 2, 3, 4, \ldots$ (i.e., all natural number larger than one) and $\lambda_r = (0, \alpha]$. The justification for doing this is discussed at the end (see 5.1).

As the energy stored increases with larger β it is of interest to investigate the volume energy density if this increase is simply due to more material being used or if there exists a more complex relationship (see Fig. 5). (As noted in the previous work [7] the cost of the NdFeB magnets is a disadvantage, thus, it is important to look at the energy density).

As can be seen (Fig. 5) there is a clear trend and a region that denotes the maximum energy density for each height of the arrays (i.e., β) and each wavelength of magnetization in the material. Note that the volume considered is the volume of the two arrays alone, $V = 2\alpha\beta\gamma$, i.e., approximately the volume of the dual configuration when this is compressed. The following observations can in generally be made:

- The maximum energy density is approximately 250 kJ/m^3 which is close (79–75 %) to the maximum energy product ($\approx$ 318–334 kJ/m^3) of N42 [6]), as discussed in [7].

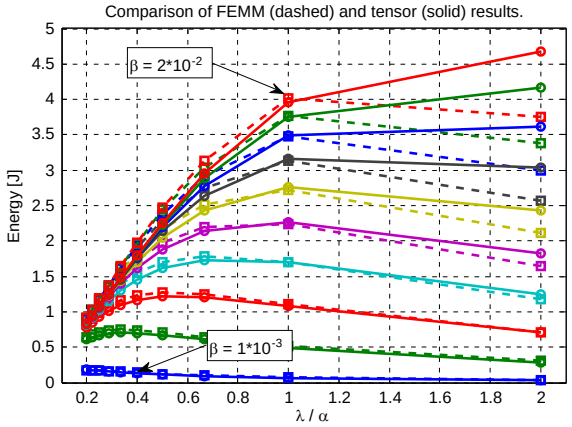

Figure 4. Comparison between numerically simulated results with FEMM (dashed lines with squares) and analytical calculations with Maxwell's stress tensor (solid lines with circles). Here, $\gamma = 1\,\text{cm}$, $\alpha = 5\,\text{cm}$ and β takes on ten equally spaced values between 1 mm and 2 cm.

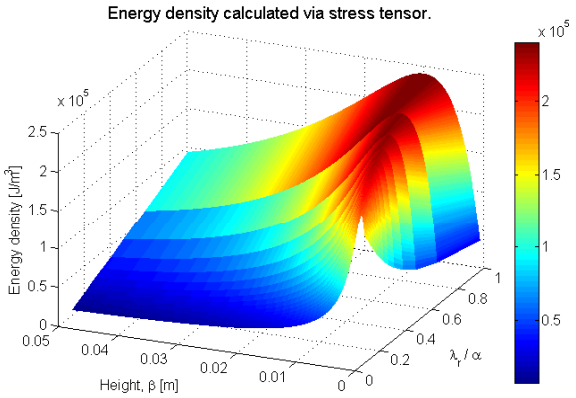

Figure 5. Using analytical calculations, a region of maximum energy density can clearly be seen. Here, $\gamma = 1\,\text{cm}$ and $\alpha = 5\,\text{cm}$.

- For large β and any $\lambda = (0, \alpha]$, the energy density doesn't reach the same maximum as for lower β.
- For a given wavelength, λ, the energy density increases with increasing β to a maximum then decreases again.

For the material considered here, i.e., $Nd_2Fe_{14}B$, the total financial cost, C, increases linearly with increasing β as $C = k(\alpha\beta\gamma)\rho$, where k is the cost/kg and ρ is the density of the material in kg/m^3 (this disregards any possible "bulk discount"). As we have seen (Fig. 5), the energy density of the dual Halbach configuration does not, for any given λ, follow a simple linear relationship, nonetheless it is clear that after the maximum point has been reached it decreases rapidly, Thus, the total cost, C, increases much more with β than the energy density does, i.e., $\frac{d}{d\beta}C \gg \frac{d}{d\beta}\frac{E}{V}$. Therefore, it is erroneous to simply increase β (or the other dimensions), i.e., larger magnets, to optimize the stored energy. For given λ, after the maximum point has been reached, it is much more cost effective to use additional material to form additional dual configurations.

5. DISCUSSION

5.1. Regarding the Relative Wavelength

Regarding the justification for using the relative wavelength, $\lambda_r = 2\frac{\alpha}{N}$, note that (19) is based on (13) which only describes the fields in the gap between the arrays (i.e., for $x = [0, \alpha]$ and $z = [0, \beta]$) and, thus, is not valid for the vertical sides. The analytical expressions used here to calculate the stored energy density via Maxwell's stress tensor (see (19)–(24)), thus, assumes a symmetry in the fields. For (19) it is assumed that the contributions from the vertical sides of the Halbach arrays are negligible in comparison to the contribution from the horizontal surfaces facing each other.

If the wavelength of the magnetization is such that $\lambda = \lambda_r$ then the ends of the array will have a direction of magnetization that will, besides polarity (i.e., sign), create similar magnetic fields. If $\lambda \neq \lambda_r$ the ends will have different field structures with "fractured" (i.e., not fully formed) poles. This as the pole pitch (pp) should be α/N (and $\lambda = 2pp$) to form complete poles and create symmetry. Therefore (19) will not accurately represent the horizontal force between the two arrays for $\lambda \neq \lambda_r$ and as can be seen in Fig. 6 it fluctuates for these. Of course, if λ is very small compared to α the effects of the ends are negligible compared to contribution from the horizontal surfaces and then even $\lambda \neq \lambda_r$ can be used (see Fig. 6).

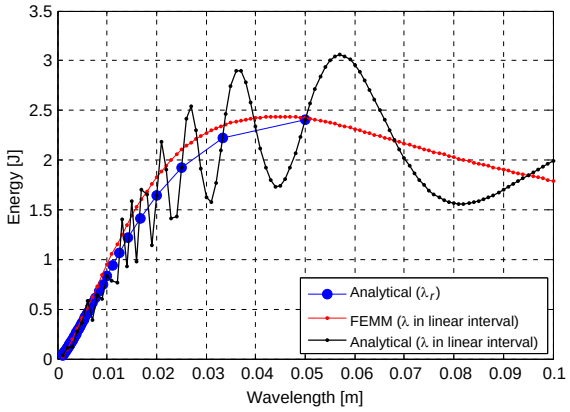

Figure 6. The tensor calculations here are not valid for all wavelengths and the solution oscillates around the correct results (using the relative wavelength or FEMM). Here, $\gamma = \beta = 1\,\text{cm}$ and $\alpha = 5\,\text{cm}$.

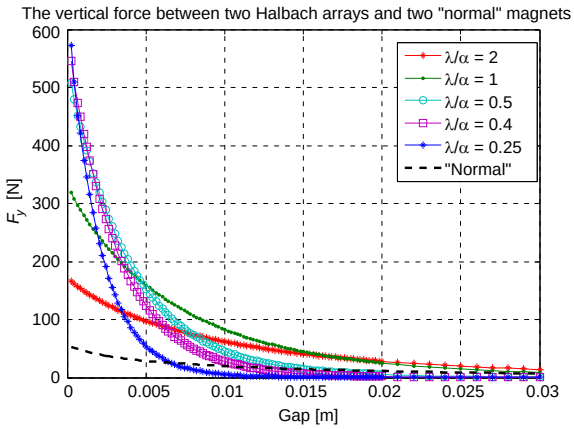

Figure 7. Using FEMM the vertical force, i.e., F_y, between Halbach arrays with different wavelengths and two "normal" magnets is obtained. Notice how the curve and, thus, integral and stored energy, for the force between two "normal" magnets is much lower. Here, $\gamma = \beta = 1\,\text{cm}$ and $\alpha = 5\,\text{cm}$ for both magnetic structures.

5.2. Regarding Internal and Shearing Forces

If the dual Halbach configuration is constructed by discrete elements (i.e., individual magnets) part of the mechanical work performed during the compression will be directed into internal forces that are directed so as to dislodge individual magnets and shearing forces that can break the individual magnets. The effects of these mentioned forces can be investigated by using simulation software (e.g., FEMM) or calculating the necessary tensor elements (T_{xy}, T_{xz} etc.) of the individual magnets. These issues were studied in the previous work (see [7]) and it was found that the shearing forces are not enough to overcome the tensile strength of the material and, thus, damage the individual magnets. The internal forces were also found to be either to small (for discrete Halbach arrays they approach zero with better discretization) to overcome the adhesive force of existing glues or zero (for continuous Halbach arrays). However, it can not be ruled out, that if the material of an individual magnet is flawed (e.g., due to construction error), the magnetic field, particularly at an edge or a corner of an individual magnet, can damage the material.

5.3. Regarding Gravity

If the direction of compression is towards earth, the mass of the upper Halbach array moving downward will, through the gravitational force, aid the compression and, thus, less work needs to be expended to store more energy. However, the same amount of work that was previously "stored for free" by the earth is subtracted from the stored energy during the release. Thus, if the motor component performing the compression and the generator component utilizing the stored energy are of equal efficiency, the effect of the gravitational force of the earth on the energy storage is a zero-sum game.

5.4. Regarding the Effect of $dB/dt \neq 0$

If the dual Halbach array is compressed quickly then $d\mathbf{B}/dt$ becomes large. This will create an electric field according to $\nabla \times E = -d\mathbf{B}/dt$ that will induce eddy currents in conducting structures in the vicinity. According to Lenz' law these currents oppose the change in flux and, thus, will create an induced magnetic field, $\mathbf{B}'$, that will be of such nature as to oppose the compression of the Halbach array. However, in [7] it was shown that the effect created by these eddy currents is negligible in this context even for very fast compressions (i.e., in the order of ms).

5.5. Comparison to Ordinary Magnets

If the two Halbach arrays in the dual configuration is replaced with two "normal" magnets with the same dimensions and maximum magnetization, M_0, in the material the force between the two arrays, and, thus, the energy stored, is much smaller than for the Halbach arrays. In Fig. 7 the force as a function of gap distance, i.e., h, is shown for different wavelengths and also for two normal magnets and it should be clear why Halbach arrays are preferred in magnetic springs.

5.6. Future Work

Although the original publication was made in 1973, Halbach arrays are still investigated and new areas of application found. As Neodymium magnets can be very strong, experimental work can be challenging especially if the individual magnets are very small. In the future, experimental work will be performed to investigate other aspects of using Halbach arrays in an energy storage system.

6. CONCLUSIONS

It is shown that the energy density has, for dimensions and wavelengths, a clear region for storing energy optimally. As the total financial cost increases faster than the energy density for increasing dimensions it is therefore unwise to simply increase the amount of material without considering the region of maximum energy density. Additional material is best used to form additional dual configurations. Also, it has been shown that, if considerations are taken with the wavelengths calculated, the Maxwell stress tensor can be greatly simplified and still be an accurate tool to calculate the magnetic forces between Halbach arrays and, thus, the energy stored when two such are moved closer.

ACKNOWLEDGMENT

This work was made possible through funding from the STandUP for Energy collaboration.

REFERENCES

1. Ter-Gazarian, A. G., *Energy Storage for Power Systems,* 2nd Edition, The Institution of Engineering and Technology, London, 2011.
2. Huggins, R. A., *Energy Storage,* Springer Science+Business Media, New York, 2010.
3. Rosen, M. A., Ed., *Energy Storage,* Nova Science Publishers Inc., Hauppauge, 2012.
4. Grijalva, S. and M. U. Tariq, "Prosumer-based smart grid architecture enables a flat, sustainable electricity industry," *IEEE PES Innovative Smart Grid Technologies (ISGT)*, 1–6, 2011.
5. Zheng, J., D. W. Gao, and L. Li, "Smart meters in smart grid: An overview," *IEEE Green Technologies Conference*, 57–64, 2013.
6. Supermagnete, Available: http://www.supermagnete.de/eng/.
7. Månsson, D., "On the suitability of using Halbach arrays as potential energy storage media," *Progress In Electromagnetics Research B*, Vol. 58, 151–166, 2014.
8. Finite Element Method Magnetics, Available: http://www.femm.info/.
9. Meeker, D., "Force on a taper plunger magnet," Available: http://www.femm.info/wiki/RotersExample.
10. Vizimag, Available at: http://www.softpedia.com/get/Science-CAD/Vizimag.shtml.
11. Mallinson, J. C., "One-sided fluxes — A magnetic curiosity?," *IEEE Trans. Magnetics*, Vol. 9, 678–682, 1973.
12. Halbach, K., "Physical and optical properties of rare earth cobalt magnets," *Nuclear Instruments and Methods in Physics Research*, Vol. 187, 109–117, Aug. 1981.
13. Wolfram Demonstrations Projects, Available at: http://demonstrations.wolfram.com/FieldsOfMagnetArray/.

14. Griffiths, D. J., *Introduction to Electrodynamics*, 3rd Edition, Prentice-Hall Inc., Upper Saddle River, 1999.
15. Shute, H. A., J. C. Mallinson, D. T. Wilton, and D. J. Mapps, "One-sided fluxes in planar, cylindrical, and spherical magnetized structures," *IEEE Trans. Magnetics*, Vol. 36, No. 2, 440–451, Mar. 2000.
16. Lang, J. H., "A comparative analysis of torque production in Halbach and conventional surface-mounted permanent-magnet synchronous motors," *IEEE Industry Applications Conference*, Vol. 1, 657–663, Oct. 8–12, 1995.
17. McDonald, K. T., "Methods of calculating forces on rigid magnetic media," *Physics Class. Ph.*, arXiv: physics/0312027, 2003.
18. WolframAlpha, Available at: http://www.wolframalpha.com/.
19. MATLAB Version R2012b, The MathWorks, Inc., Natick, Massachusetts, United States, 2012.